IVYSPRING INTERNATIONAL PUBLISHER

Theranostics

2019; 9(2): 526-536. doi: 10.7150/thno.30779

Research Paper

Stimuli-Responsive Nanotheranostics for Real-Time Monitoring Drug Release by Photoacoustic Imaging

Zhen Yang[1,2,4*], Jibin Song[3*], Wei Tang[4*], Wenpei Fan[4], Yunlu Dai[4], Zheyu Shen[4], Lisen Lin[4], Siyuan Cheng[4], Yijing Liu[4], Gang Niu[4], Pengfei Rong[1,2], Wei Wang[1,2]✉, Xiaoyuan Chen[4]✉

1. Cell Transplantation and Gene Therapy Institute, The Third Xiangya Hospital, Central South University, Changsha, Hunan, China.
2. Engineering and Technology Research Center for Xenotransplantation of Human Province, Changsha, Hunan, China.
3. MOE Key Laboratory for Analytical Science of Food Safety and Biology College of Chemistry, Fuzhou University, Fuzhou 350108, China
4. Laboratory of Molecular Imaging and Nanomedicine (LOMIN), National Institute of Biomedical Imaging and Bioengineering (NIBIB), National Institutes of Health (NIH) Bethesda, Maryland 20892, United States

*Z. Yang, J. Song and W. Tang contributed equally to this work

✉ Corresponding authors: E-mail: cjr.wangwei@vip.163.com; E-mail: shawn.chen@nih.gov

Received: 2018.10.18; Accepted: 2018.12.04; Published: 2019.01.01

Abstract

Molecular photoacoustic imaging (PA) is a promising technology to understand tumor pathology and guide precision therapeutics. Despite the capability of activatable PA probes to image tumor-specific biomarkers, limitations in their molecular structure hamper them from effective drug delivery and the drug release monitoring. Herein, we developed a perylene diimide (PDI) based theranostic platform that provides noninvasive PA imaging signals to monitor tumor-specific pH-responsive drug release.

Methods: we first designed and synthesized an acid-responsive amine-substituted PDI derivative. The pH sensitive properties of the PDI was demonstrated by density functional theory (DFT) calculations, UV-vis experiments and PA studies. The theranostic platform (THPDINs) was fabricated by self-assembly of the acid-responsive PDI, a pH irrelevant IR825 dye, and anti-cancer drug doxorubicin (DOX). The PA properties in various pH environment, drug delivery, cytotoxicity, cell uptake, ratiometric PA imaging and anti-tumor efficacy of the THPDINs were investigated *in vitro* and *in vivo* by using U87MG glioma cell line and U87MG tumor model.

Results: We found that our designed PDI was sensitive to the tumor specific pH environment, reflected by absorbance shift, PA intensity and aggregation morphology changes in aqueous solution. The as-synthesized pH sensitive PDI acted as a molecular switch in the THPDINs, in which the switch can be triggered in the mild acidic tumor microenvironment to accelerate DOX release. Meanwhile, the DOX release could be monitored by ratiometric PA imaging.

Conclusions: We developed a multifunctional PDI based theranostic platform for noninvasive real-time ratiometric PA imaging of tumor acidic pH and monitoring of drug release in living mice simultaneously. This strategy will shed light on the development of smart activatable theranostic nanoplatforms and will significantly advance the application of PA theranostics in biology and medicine.

Key words: photoacoustic imaging, ratiometric imaging, drug delivery, pH-responsive, theranostics

Introduction

Nanotheranostics, interwoven with both diagnostic and therapeutic functions, can achieve accurate tissue targeting and optimal treatment efficacy for many diseases, especially for cancer management [1, 2]. As for cancer diagnosis, PA imaging collects photon-triggered acoustic signals and non-invasively constructs tumor images with reasonably high resolution [3-9]. In particular, ratiometric PA imaging based on activatable probes, with ultrasensitive detection of tumor biomarkers and minimal interference of endogenous PA contrast, can achieve much higher signal-to-noise ratio than conventional

"always on" probes [10-14]. Recently, a variety of ratiometric PA probes have been successfully developed and applied for accurate detection of reactive oxygen species (ROS), hypoxia, and pH in the tumor microenvironment (TME), which highly promoted the application of ratiometric PA imaging in biomedicine [10, 15, 16].

For cancer therapy, chemotherapeutics, such as doxorubicin (DOX), gemcitabine and cisplatin, have shown effective antitumor efficacy in the clinic [17-19]. In order to simultaneously maximize the therapeutic effectiveness and minimize the systemic toxicity of free chemotherapeutics, a number of functional nanocarriers, such as polymer micelles and nanovesicles [20-22], have been designed for tumor-specific drug delivery. Especially, the nanocarriers featured with TME stimuli (*e.g.*, higher ROS level, reducibility, hypoxia, or acidity)-responsive drug releases have attracted extensive attention. As we know, acidity is a general hallmark of cancer due to its inordinate metabolism. The pH of normal tissue is about 7.3–7.5, whereas those of tumor tissue and their endosomes and lysosomes are 6.5–7.2 and 4.0–6.0, respectively [23-26]. The pH gradient allows for the design of acidity-responsive drug release system for precise drug release and on-demand chemotherapy. Furthermore, the detection of acidic TME with pH activatable imaging probes is beneficial to effectively monitor the drug release, based on the molecular imaging signal changes [27-33]. Nowadays, the development of activatable PA probes is still at the preliminary stage, which can only be used for imaging tumor biomarkers, but are seldomly used to monitor the drug release, due to the limitations of the molecular structure of PA probe. Therefore, it is of essential importance to develop smart nanotheranostics that allow simultaneous acidic TME-responsive ratiometric PA imaging and real-time cancer chemotherapy monitoring.

Recently, organic semiconducting nanoparticles have received extensive interests due to their excellent PA contrast performance [34-42]. These nanoparticles consist of soft electron-rich materials with strong near-infrared (NIR) absorption, such as conjugated polymers and π-conjugated small molecules. PDI is a typical kind of small semiconducting molecules that can be used for PA imaging for detecting tumor, thrombi and lymph nodes [43-46]. The lone pair electrons of amine act as an electron donor to the acceptor PDI, which causes a redshift of its absorption from 530 nm to 680 nm for excellent PA contrast. On the contrary, the compromise of electron donation from amine group to PDI aromatic ring is expected to induce a blue shift of absorption and quenching of PA signals in the near-infrared region [47]. Herein, we report a pH-sensitive nanotheranostic agent consisting of an acid-responsive amine-substituted PDI derivative, a pH insensitive NIR dye (IR825), and an anti-cancer drug DOX (**Figure 1**). Based on charge transfer mechanism, the acidity-responsive pH indicator PDI was designed by introducing N-methyl piperazine to PDI bay position to realize a strong 680 nm absorption under neutral condition, which can be weakened according to the degree of protonation of the tertiary amine group at lower pH. Moreover, the π plane and hydrophobicity of PDI facilitate the efficient encapsulation of hydrophobic DOX [48]. The protonation of PDI also can speed up the DOX release by increasing the hydrophilicity of PDI. Besides, the hydrophobic IR825 with pH irrelevant absorption peak at 825 nm can be encapsulated by PDI, which acts as an internal reference of the ratiometric PA probe. Therefore, the pH-sensitive nanotheranostic agent could not only specifically image the tumor region and map its pH, but also allow on-demand drug release to effectively inhibit tumor growth.

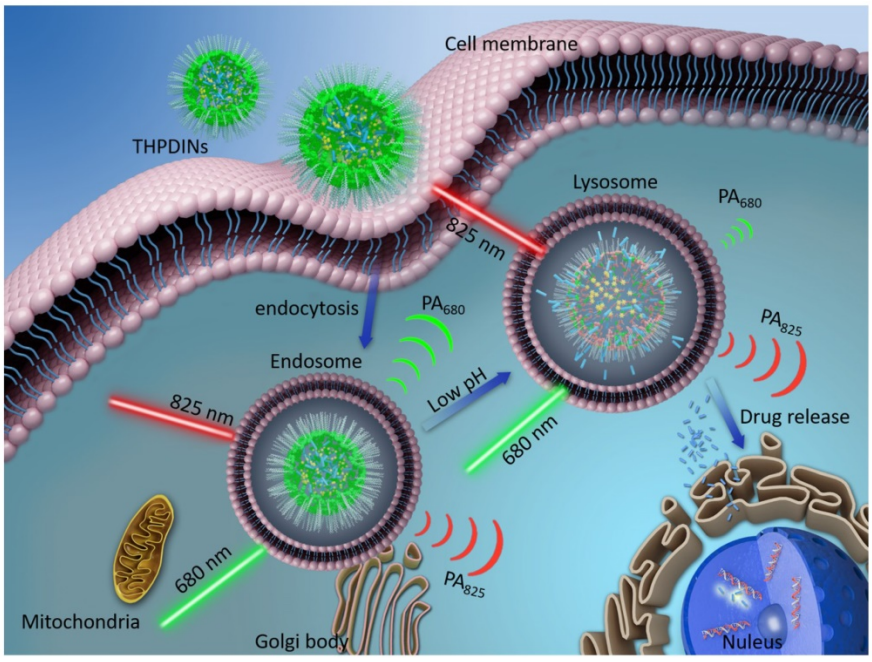

Figure 1. The illustration of internalization of a theranostic platform−THPDINs. Upon internalization, low pH environment induces a protonation reaction of the HPDI, achieving simultaneously ratiometric pH imaging and DOX release monitoring.

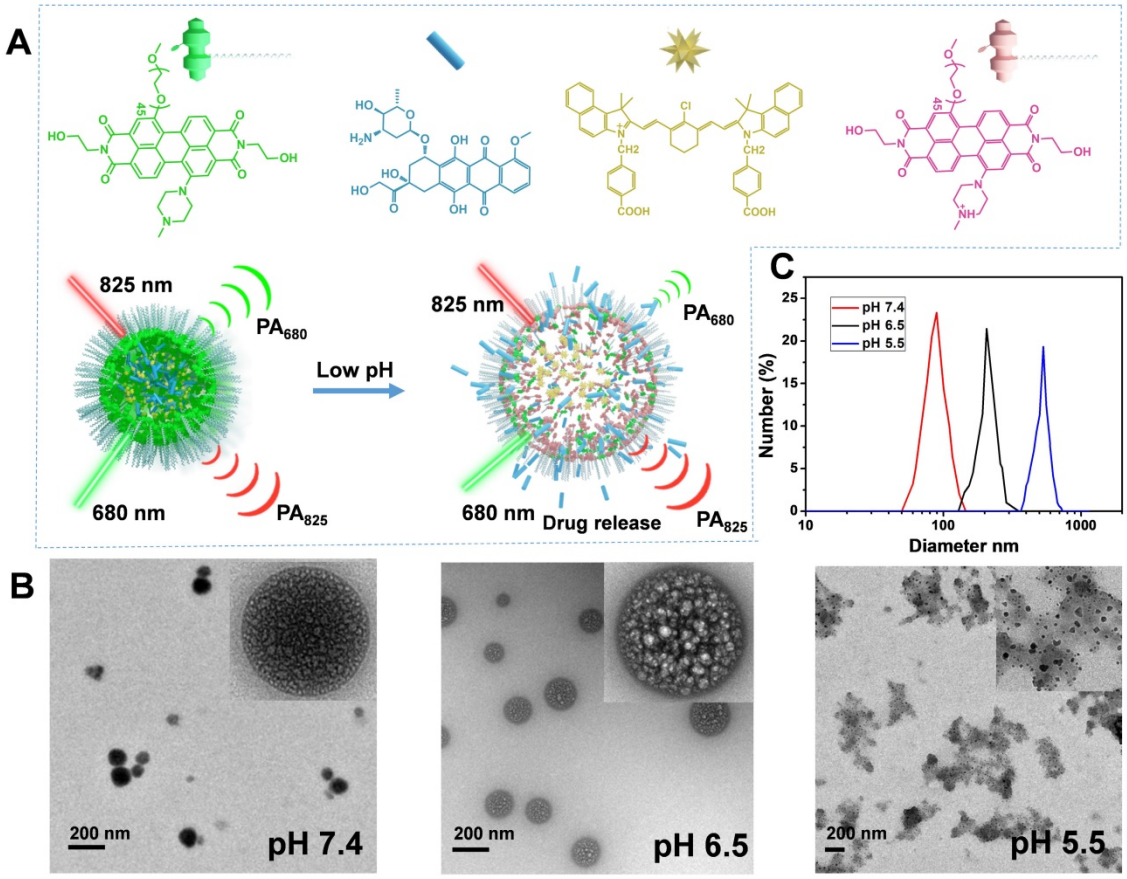

Figure 2. Characterization of the THPDINs theranostic platform. (A) Schematic illustration of the sensing and drug releasing mechanism of THPDINs. The THPDINs is self-assembled with a pH-sensitive HPDI (green), a pH-inert IR825 (gold), and an anticancer drug of DOX (blue). At low pH, the HPDI will be protonated (pink), inducing a loosened nanostructure that could trigger the release of the encapsulated DOX accompanied by PA signals vanishing at 680 nm. Meanwhile, the chemical structure of IR825 and its characteristic PA signal at 825 nm retain the same. Therefore, the DOX release process could be monitored by a ratiometric PA imaging at PA_{825}/PA_{680}. **(B)** TEM images and **(C)** DLS data indicate diameters of the THPDINs in buffer solutions with different pH values.

Results and Discussion

Fabrication of PDI based theranostics

In this study, the HPDI and APDI were synthesized to compare their pH sensitivity and drug release characteristics (**Figure S1-S10**). The HPDI and APDI own different substituents on the PDI's aide position, which are hydroxyl groups and alkyl chains, respectively. The hydrophobic group of the amide position of PDI is expected to reduce the PDI's pH sensitivity and inhibit premature release of the encapsulated drugs. In our experiments, the HPDI based nanoagent was shown to be an ideal platform for concurrent ratiometric PA imaging and drug release monitoring. THPDINs, consisting of DOX, HPDI (a pH indicator), and IR825 dye (a pH inert PA matrix), was synthesized by a nanoprecipitation method (**Figure 2a**). These three components could be self-assembled into a nanoparticle through hydrophobic interactions and π-π stacking at neutral pH. After the assembly, the PEG_{2000} in the amphiphilic PDI structure endows the theranostic nanoagent with high water solubility and biocompatibility. TEM images revealed the morphology evolution of the THPDINs at different pH values (**Figure 2b**). When the pH decreased from 7.4 to 6.5, the quaternized PDI aggregates changed from tight to loosened structures, inducing a relatively bigger particle size. At pH 5.5, a majority of DOX and PDI in the particle turned out to be hydrophilic, resulting in deformation of the nanoparticles. DLS showed that the average diameter of the THPDINs changed from 90 ± 6 nm to 184 ± 15 nm and finally to 519 ± 30 nm (**Figure 2c**). The THPDINs was stable in PBS solution (**Figure S11**). In comparison with THPDINs, TEM and DLS results of the APDINs (**Figure S12-S13**) retained a relatively stable nano size and spherical morphology at pH 5.5, which indicated that the alkyl chain along with π plane of PDI caused serious aggregation and lowered the pKa constant of the alkyl-based PDI structure. Thus, these results suggest that HPDI has high sensitivity of morphology changes in response to a low pH, presumably due to the fact that hydroxyl group increased the hydrophilicity of the perylene

core, promoted the hydrogen proton access to the tertiary amine on the bay position, and therefore boosted the quaternization of PDI under weak acidity. The high pH sensitivity featured HPDI a unique platform that can sense low pH and simultaneously release its encapsulated drugs.

Photophysical Properties of PDI based theranostics

To better understand the role of protonation of the N-methylpiperazine group in the HPDI, density functional theory (DFT) calculations were conducted based on Gaussian 09 [49]. The geometries of the pH-sensitive PDI structure and the reaction product of PDI with proton were optimized by B3LYP method basis sets. The optimized geometries showed planar perylene diimide cores on ground-stated geometry (S0), which facilitated π-π stacking and drug loading in water. In the molecular structure of N-methylpiperazine based PDI, the HOMO and LUMO frontier molecular orbitals were delocalized throughout the PDI core (**Figure 3a**). However, after protonation of N-methylpiperazine, the LUMO of the PDI structure was localized on the protonated N-methylpiperazine, which led to a non-conjugated electronic cloud on PDI core. This disturbed electronic cloud might explain the blue shift of the UV–vis absorption after protonation of PDI structure.

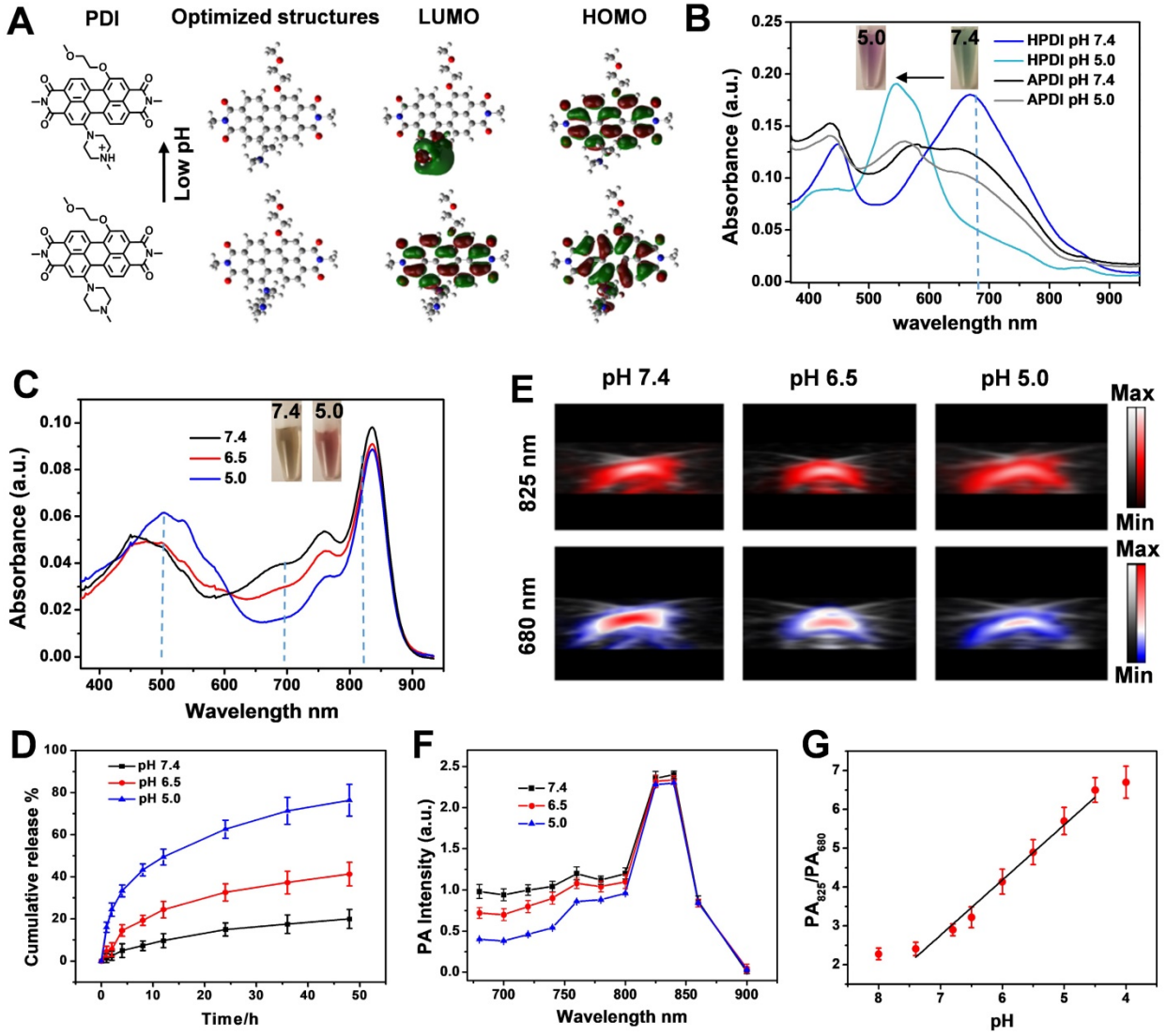

Figure 3. Characterization of the photophysical properties of the acidity-sensitive PDI structure and its based THPDINs. (A) Chemical structure, geometry-optimized structure, and HOMO and LUMO wave functions before and after protonation of the pH-sensitive PDI (The methyl chains were modified to amide position of PDI for simplicity). **(B)** UV–vis absorption spectra variation of HPDINs and APDINs at pH 7.4 and 5.0. **(C)** UV–vis absorption spectra of THPDINs and **(D)** Release profiles of DOX from THPDINs at buffer solutions with different pH (Inset picture showed THPDINs solutions at pH 7.4 and 5.0). **(E)** Representative PA images of the THPDINs solution at 680 and 825 nm. PA specific capillary tubes loading different THPDINs solution at different pH for the PA imaging tests at 680 and 825 nm, respectively. The solutions are indicated in pseudo color. **(F)** Representative PA spectra ranging from 680 to 900 nm of the THPDINs under different pH. **(G)** Quantification of the ratiometric PA signals (PA_{825}/PA_{680}) of the THPDINs as a function of various pH from 4.0 to 8.0.

The absorption of the PDIs and PDI-based ratiometric PA imaging platform was systematically investigated. The absorption of the as-synthesized HPDI and APDI were first measured in different solvents (**Figure S14**), which showed strong absorption peaks at around 700 nm and a redshift tendency in the polar solvents. In a neutral solution (**Figure S15**), the amphiphilic HPDIs formed nanoparticles with strong absorption at 680 nm, which was an appropriate excitation wavelength for PA imaging. To fabricate the ratiometric PA probe, we selected IR825 dye as a standard probe with no absorption at 680 nm. The IR825 showed pH-independent and robust absorption at around 825 nm within the pH range of 3.0−8.0 (**Figure S16**), which has also been verified by previous reports [50-52]. The optical properties of the PDI nanoparticles were measured at different pH values in PBS. The absorption of HPDI nanoparticles (HPDINs) at 680 nm showed high sensitivity to pH change from 7.4 to 5.0, whereas APDINs showed no response to acidity (Figure 3b). These observations demonstrated that the hydrophobicity on the amide position of APDI was a key factor for repelling accessibility of water molecules to the bay position and inhibiting the protonation of N-methylpiperazine. The protonation of HPDI was also demonstrated by the reversible zeta potential between pH 7.4 and 5.0 (**Figure S17**). Therefore, HPDI was chosen for pH-responsive PA imaging. After the encapsulation of the hydrophobic IR825 and DOX, the absorption of the THPDINs was investigated (**Figure 3c**). With decreasing pH, the absorption peak descended at 680 nm but remained the same at 825 nm. Based on the spectra, we also observed that the absorption at 500 nm increased, and the color of the solution changed from brown to red (shown in the inset pictures) with the pH decreased from 7.4 to 5.0, which illustrated that the DOX was also protonated at low pH environment and changed from aggregation to dispersion state. Therefore, based on the pH-responsive UV-vis absorption spectra of THPDINs, the ratio of Ab_{825}/Ab_{680} was quantified to be a function of pH value (**Figure S18**). The ratiometric absorption signal of Ab_{825}/Ab_{680} at pH 5.0 was 2.21-fold and 1.76-fold higher than those at pH 7.4 and 6.5, respectively. This indicated that the well-designed ratiometric probe could accurately differentiate the normal physiological pH (7.4) and the pathological tumor pH (5.0 and 6.5) (**Figure 3c**).

The quantitative determination of drug release was obtained by measuring the UV-vis spectrum of DOX outside dialysis tubes (**Figure 3d**). The drug loading content of DOX was quantified to be as high as 18.4% and 20.6% to HPDINs and APDINs, respectively. The fluorescence intensity of DOX at pH 7.4 was very weak, which was attributed to the aggregation-induced fluorescence emission quenching and fluorescence resonance energy transfer (FRET) from DOX to PDI [53]. However, the fluorescence of DOX was significantly recovered upon acidification of the solution to pH 5.0 (**Figure S19**). Compared with the DOX release profile of THPDINs, the control group of DOX-loaded APDINs showed a prolonged DOX release (**Figure S20**), which maybe because the strong π-π stacking of the planar PDI cores together with the hydrophobic alkyl side chains effectively trapped DOX in the APDINs. Therefore, the ratiometric absorption of PDI and IR825 could reflect the DOX release at different pH solutions. The performance of THPDINs in PA imaging of pH was evaluated in the solutions of various pH values. The PA/US images of the THPDINs solutions were recorded at the wavelengths of 680 nm and 825 nm at three biologically relevant pH values (**Figure 3e**). The PA intensity at 825 nm was stable regardless of pH changes, while the relative intensity at 680 nm decreased from around 1 to 0.4 when pH changed from 7.4 to 6.5 and 5.0 (**Figure 3f**). A ratiometric PA value (PA_{825}/PA_{680}) was calculated based on the ratio of PA intensities at the two wavelengths. The ratiometric PA signal at pH 5.0 was 5.7 ± 0.35, which was around 1.77- and 2.38-fold higher than those at pH 6.5 (3.22 ± 0.27) and 7.4 (2.4 ± 0.17), respectively. From the drug release curve of THPDINs, we could obtain the drug release of 15%, 32%, and 62%, which quantitatively correspond to the ratiometric PA signals under pH 7.4, 6.5, and 5.0 at 24 h, respectively. Good linearity between the ratiometric signal and pH was presented within the range of pH 7.4 to 5.0 (**Figure 3g**), indicating that the fitted line can be potentially used as the standard curve to quantify pH *in vivo*.

In vitro Drug Delivery Studies

To observe the DOX release from THPDINs *in vitro*, the confocal fluorescence images were acquired after incubation of THPDINs with U87MG cells for 0.5, 2 or 6 h. Upon incubation with THPDINs for 0.5 and 2 h, red fluorescence signal mainly appeared in the cytoplasm of U87MG cells, indicating that the THPDINs were gradually uptaken by cells and the encapsulated DOX was protonated (**Figure 4a**). With the extension of the culture period to 6 h, the DOX was localized in the nucleus and the red fluorescence intensity in cells remarkably increased as well (**Figure S21**). The results confirmed that the pH-responsive PDI theranostic platform could be uptaken by U87MG cells and the released DOX can arrive at the nucleus. The quantification of DOX intensity in the cells at different time points also demonstrated the extensive DOX release in cancer cells (**Figure 4b**). The cytotoxic

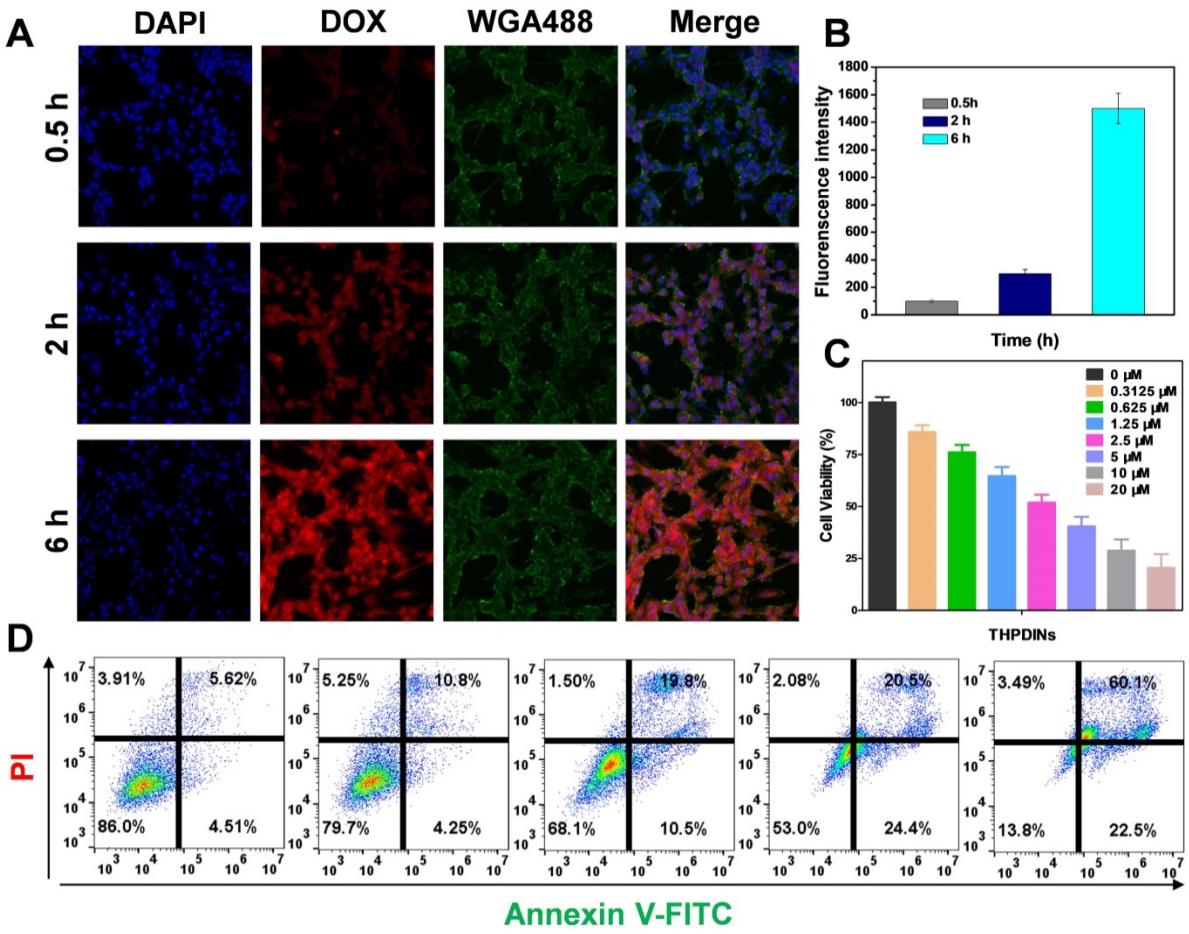

Figure 4. Investigation of *in vitro* therapeutic effect of THPDINs. (A) CLSM images (Scale bar, 50 μm) and **(B)** quantitative DOX intensities of the U87MG cells incubated with the THPDINs for 0.5, 2 and 6 h. **(C)** Cytotoxicity of U87MG cells with different treatments: THPDINs with various DOX concentration. **(D)** The apoptosis of U87MG cells analyzed by flow cytometry, the cells were treated with THPDINs in various DOX concentration (0, 0.3125, 1.25, 5, 20 μM).

effect of the THPDINs on U87MG cells was further evaluated by using MTT assay (**Figure 4c**). APDINs and HPDINs showed no toxicity to U87MG cells (**Figure S22**), indicating good biocompatibility of the PEG_{2000} linked PDIs. Also, we detected apoptosis in U87MG cells after the treatment with THPDINs. As a result, an increased percentage of apoptotic cells was found with the concentration increased (**Figure 4d**), suggesting promising application potentials of our designed THPDINs platform for cancer therapy.

In vivo PA investigation of PDI based theranostics

To demonstrate the feasibility of THPDINs for the ratiometric PA imaging of tumor pH *in vivo*, THPDINs (10 μL, 5 mg mL^{-1}) were first locally administered into mice normal tissue after changing the subcutaneous pH value *via* injection of 25 μL of citric buffer (pH 5.0) or $NaHCO_3$ solution (pH 8.0). PA signals at 680 and 825 nm were measured at the two artificial pH environments (**Figure S23**). The PA signal at 825 nm remained unchanged at different pH values. However, the PA signal at 680 nm was much weaker at pH 5.0 than that at pH 8.0, indicating that PDI was protonated at low pH. The specific ratiometric signal change could easily be distinguished from the PA images. ΔPA was defined as true PA signal of probes with a deduction of the endogenous PA intensity to minimize the tissue interference. The ratiometric PA signal ratio ($\Delta PA_{825}/\Delta PA_{680}$) of the THPDINs at pH 5.0 (4.8 ± 0.5) was about 2-fold higher than that at pH 8.0 (2.4 ± 0.4). The significantly intensified ratiometric PA signal of THPDINs in acidic tissue environment suggested its ability to probe the tumor pH. To visualize the ratiometric PA image of tumor pH and trace chemotherapeutics *in vivo*, THPDINs (200 μL, 5 mg mL^{-1}) were intravenously injected into the U87MG tumor-bearing mice. The PA images at the wavelengths of 680 and 825 nm were performed using pseudo green and red colors, respectively (**Figure 5a**). The PA signal increment at 825 nm (ΔPA_{825}) in the THPDIN-treated mice was substantially increased owing to the EPR effect of the theranostics. However, the increase of ΔPA_{680} was much less than that of ΔPA_{825}, which was attributed to the acidic TME-induced protonation of the HPDIs

(**Figure 5b**). As seen from the obtained PA images of the treated mice, the ratiometric PA signal ratio ($\Delta PA_{825}/\Delta PA_{680}$) gradually increased and reached its maximum at ~24 h post-injection (4.36 ± 0.54, **Figure 5c**), which was ~1.74-fold higher than that at 2 h post-injection (2.5 ± 0.23). These data not only validated that the theranostic THPDINs could reflect the pH in tumor region but also indicated that the ratiometric imaging could monitor the drug release *in vivo*.

In Vivo Therapeutic Efficacy of PDI Based Theranostics

The promising PA imaging results encouraged us to further evaluate the antitumor efficacy of the THPDINs. U87MG tumor mice were randomly divided into five groups, which were administered with PBS, free DOX, HPDINs, DOX-loaded APDINs, and THPDINs, respectively. The mice treated with PBS, HPDINs, and DOX-loaded APDINs exhibited rapid tumor growth (**Figure 6a**), indicating negligible tumor inhibition by using those control materials. The free DOX treated mice showed a slower tumor growth rate in comparison to the PBS control. THPDINs could effectively inhibit the tumor growth and showed higher anticancer efficacy than free DOX *in vivo*. The survival of the THPDINs-treated mice was also much longer than the other control groups (**Figure 6b**). No significant body weight loss was observed during the treatment (**Figure S24**), indicating that the theranostic platform of THPDINs exhibited high biocompatibility and caused little to no side effects. In addition, the H&E stained tumor sections showed extensive tumor cell apoptosis and necrosis after the treatment of THPDINs, which further validated the outstanding anticancer effect of the THPDINs (**Figure 6c**). These results suggested that DOX-loaded pH-responsive PDI produced remarkable inhibitory effect on tumor growth. H&E staining of the heart, liver, spleen, lung and the kidneys of the mice in these experiments did not show any necrosis 7 days after the material injections (**Figure S25**). These results demonstrated that the treatment of THPDINs did not observe acute toxicity to the mice.

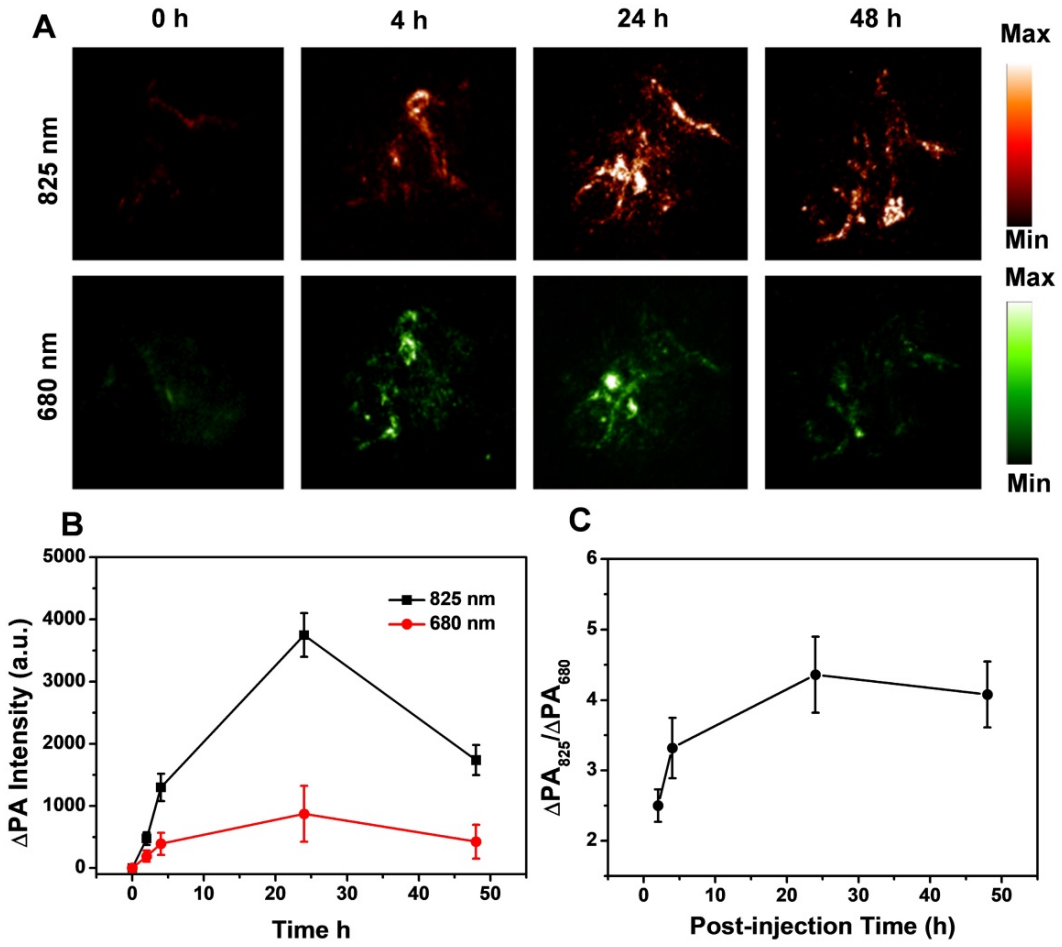

Figure 5. ***In vivo*** **PA imaging of tumor pH. (A)** Representative PA images of a subcutaneous U87MG tumor in a nude mouse after intravenous administration of the THPDINs at post-injection time 0, 4, 24, 48 h. **(B)** Quantification of the PA intensity increment at 680 (ΔPA_{680}) and 825 nm (ΔPA_{825}) as a function of the post-injection time of the THPDINs. **(C)** Ratiometric PA signals ($\Delta PA_{825}/\Delta PA_{680}$) as a function of post-injection time. The error bars showed three separate standard PA tests (n = 3).

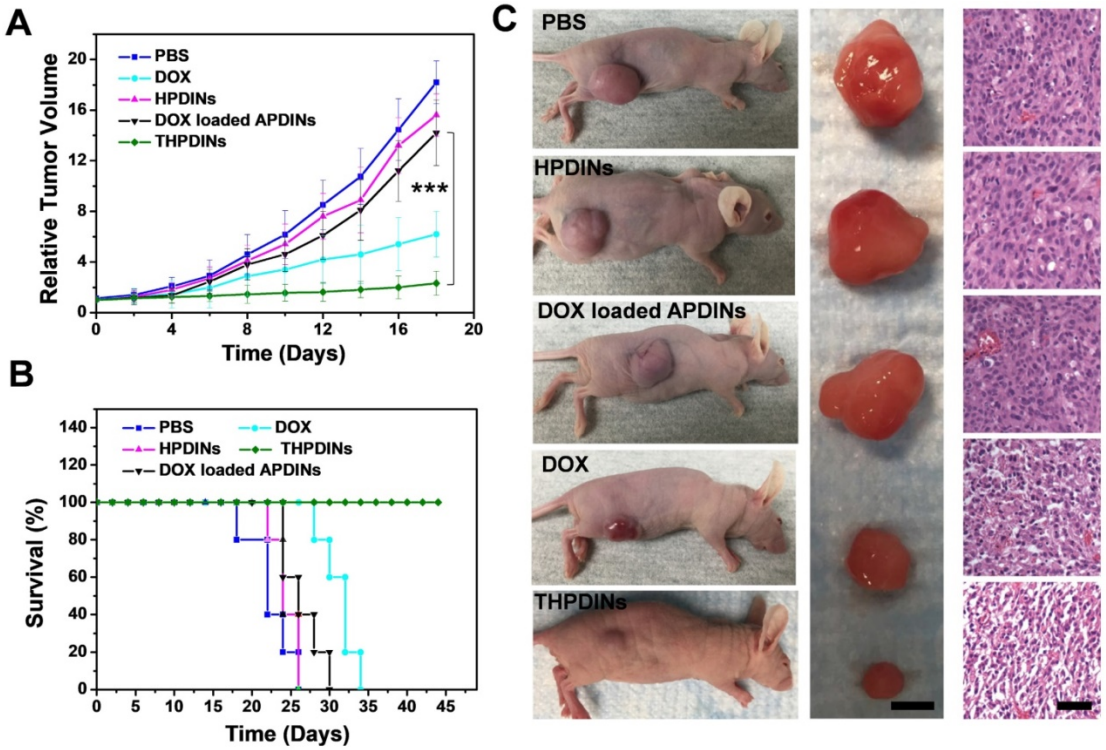

Figure 6. ***In vivo*** **cancer therapeutic efficacy of theranostic platforms. (A)** Xenograft U87MG tumor volume growth curves in different treatment groups: PBS, free DOX, HPDINs, DOX loaded APDINs and THPDINs. **(B)** The survival rate curves of the treated mice with various treatments of PBS, free DOX, HPDINs, DOX loaded APDINs and THPDINs. **(C)** Representative photographs of tumor bearing mice, resected U87MG tumors (scale bar, 0.5 cm), and H&E stained images (Scale bar, 0.1 cm) in different treatment groups on day 18. Compared with the control groups, the tumor treated by THPDINs showed strong therapeutic efficacy. ***, $P < 0.001$.

Conclusions

In conclusion, we developed a multifunctional nanotheranostics for concurrent noninvasive real-time ratiometric PA imaging of tumor acidic pH and monitoring of drug release in living mice. The intriguing HPDI structures were successfully designed and systemically characterized. In the acidic solution, HPDI structure was protonated and went through a hydrophilic structural change to release the encapsulated DOX accompanying with PA signal changes. By further incorporation of a pH inert IR825 dye, a ratiometric PA theranostic platform can be fabricated through self-assembly of the three components. Our designed theranostic platform provides a concept that noninvasive PA imaging signals could monitor tumor-specific pH-responsive drug release. This strategy sheds light on the development of smart activatable theranostic nanoplatforms and will greatly advance the application of new generation of PA theranostics in biology and medicine.

Experimental Section

Materials and Characterization

Chemicals

All solvents and chemicals were purchased from Sigma-Aldrich (St. Louis, MO), and used without further purification. Pure water was supplied by Milli-Q Plus System (Millipore Corp., Bedford, MA).

Methods

^{1}H NMR spectra were obtained on Bruker Ultra Shield Plus 300 MHz, using $CDCl_3$, DMSO-6d as the solvent. The nanoparticles morphology was obtained by TEM images (a JEOL TEM 2010 electron microscope at an acceleration voltage of 100 kV). UV–vis spectra were obtained on a SHIMADZU UV–2501 spectrophotometer. DLS was performed on the Malvern Zeta Sizer Nano S. Confocal laser scanning microscopy was conducted on a Zeiss LSM 780. PA spectra and PA/US images were performed by a LAZR instrument (Visualsonics, 2100 High-Resolution Imaging System). Endra Nexus128 PA tomography system (Endra Inc., Ann Arbor, Michigan) was also used in this study.

Preparation of PDI nanoparticles (PDINs)

Amphiphilic PDIs was dissolved in THF (2 mL). The PDINs was prepared by dropping excess water (5 mL) into the solutions under sonication at 40 °C. THF was removed through slow evaporation at 50 °C and the resultant PDINs were collected and concentrated by ultrafiltration.

Preparation of THPDINs (DOX loaded APDINs using the same procedure)

4 mg DOX and 12 mg HPDI was firstly deprotonation by dissolving in THF/MeOH (100:1, volume ratio) with equivalent triethylamine. The IR825 THF solution was prepared in advance, briefly, 1 mg IR825 was firstly dissolved in 10 μL MeOH to get a suspension liquid. Then 5 mL THF was added to the suspension with strong sonication. Finally, the clarified IR825 solution was obtained. Those prepared THF/MeOH solution of HPDI (12 mg), IR825 (0.05 mg) and DOX (4 mg) were mixed to 2 mL. The nanoparticles were formed by dropping 5 mL water into above THF/MeOH solution. Subsequently, THF/MeOH was removed by slow evaporation at 50 °C, and the THPDINs solution was condensed by Amicon Ultra centrifugal filters (10 kDa). The final nanoparticles were concentrated in 10 mmol PBS and filtered through a 0.22 μm filter. The THPDIN solution was lyophilized and resolved in DMF to evaluate the loading content. The absorption of DOX was obtained by subtracting the absorption of PDI at 500 nm. The loading content was calculated by the following equation: weight of encapsulated DOX/weight of DOX loaded PDI nanoparticles*100 %. Weight of encapsulated DOX was measured by UV-vis spectra.

In vitro drug release property of DOX loaded PDI solution

1 mL DOX loaded PDI solution was filled into dialysis tubing (MW, 2500), which was then sealed and immersed in 5 mL PBS buffer (pH 7.4) and sodium acetate buffer (pH 5.0), respectively. The dialysis system was incubated in water bath at 315 K with vigorous stirring. At designated time points, the buffer was extracted to quantify the amount of released DOX, and then another 5 mL fresh corresponding buffer was supplemented to the dialysis system for further study. The concentration of released DOX was measured by UV-Vis absorption spectra.

In vitro cytotoxicity of THPDINs

MTT assay was performed to investigate the cytotoxicity of PBS, free DOX, HPDINs, DOX loaded APDINs and THPDINs. U87MG cells were seeded on a 96-well plate at a density of 5,000 cells per well and cultured at 37 °C, 5% CO_2 for 24 h. Then, culture media was replaced by media containing different concentrations of PBS, free DOX, HPDINs, DOX loaded APDINs and THPDINs. The cells treated with different solution were incubated at 37 °C, 5% CO_2 for 48 h. Then, the medium was replaced with 100 μL fresh medium and 10 μL MTT (5 mg mL^{-1} in PBS) for another 4 h incubation. The MTT medium was replaced with DMSO (100 μL) and the absorbance of each well was measured at 570 nm by microplate reader.

Cellular imaging by confocal microscopy

The U87MG cells were seeded at a density of 25,000 cells per well in 8-well Lab-Tek cover glass slides. THPDINs were incubated with cells for 0.5, 2 and 6 h, followed by washing with PBS. Cells were stained with mounting medium with DAPI and WGA488 for 30 min. The stained cells were observed with a confocal fluorescence microscope (Zeiss LSM 780).

In vitro and *in vivo* PA imaging

For the *in vitro* experiments, the PDI solutions at different concentrations were filled into polyethylene 50 capillaries. A container was filled with 1% agarose gel to bury the tubes mentioned above testing under Visual Sonic Vevo 2100 LAZR system (40 MHz, 256-element linear array transducer), the wavelength of the laser was chosen from 680 nm to 900 nm. For the *in vivo* local PA imaging, 25 μL of citric buffer (pH 5.0) or $NaHCO_3$ solution (pH 8) pretreated the subcutaneous muscle with different pH. Then, THPDINs solution was injected into that environment to obtain ratiometric PA signals by Visual Sonic Vevo 2100 LAZR system. The PA imaging of tumor environment was obtained by *i.v.* injection of THPDINs to U87MG tumor bearing mice under Endra Nexus128 PA tomography system. The quantified PA intensities were obtained from the ROIs.

In vivo cancer therapy

All procedures were conducted following a protocol approved by the National Institutes of Health Clinical Center Animal Care and Use Committee (NIH CC/ACUC). U87MG tumor-bearing mice were prepared by inoculating with U87MG cells (3×10^6) on the flank of each female nude mouse. These mice were divided into five groups for treatment with PBS, free DOX, HPDINs, DOX loaded APDINs and THPDINs, respectively. The mice were treated with *i.v.* injection of different samples every other day for a total of three times. The tumor sizes and body weights were measured every two days, and the tumor volumes were calculated according to the formula: volume= $LW^2/2$, (L and W refer to the length and width of the tumor, respectively).

Abbreviations

PA: photoacoustic imaging; PDI: perylene diimide; DOX: doxorubicin; ROS: reactive oxygen species; TME: tumor microenvironment; NIR:

near-infrared; IR825: NIR dye 825; PBS: phosphate buffered saline; HPDI: hydroxyl based PDI; APDI: alkyl-based PDI; HPDINs: HPDI nanoparticles; THPDINs: PDI based theranostic nanoagents; EPR: enhanced permeability and retention; TEM: transmission electron microscopy; DLS: dynamic light scattering; APDINs: the DOX loaded APDI nanoparticles; DFT: density functional theory; S0: ground-stated geometry; PBS: phosphate buffered saline; FRET: fluorescence resonance energy transfer; H&E: hematoxylin and eosin; ROIs: region of interests.

Supplementary Material

Supplementary figures.
http://www.thno.org/v09p0526s1.pdf

Acknowledgments

This work was financially supported by the Intramural Research Program (IRP) of the NIBIB, NIH, and the National Natural Science Foundation of China (No. 81771827, 81471715). We thank Dr. Vincent Schram in the NICHD Microscopy Imaging Core for technical support. We are also grateful to Xiangchun Li of Nanjing University of Posts and Telecommunications for density functional theory (DFT) calculations by Gaussian 09.

Competing Interests

The authors have declared that no competing interest exists.

References

1. Fan W, Yung B, Huang P, Chen X. Nanotechnology for multimodal synergistic cancer therapy. Chem Rev. 2017; 117: 13566-638.
2. Dai Y, Xu C, Sun X, Chen X. Nanoparticle design strategies for enhanced anticancer therapy by exploiting the tumour microenvironment. Chem Soc Rev. 2017; 46: 3830-52.
3. Lyu Y, Zhen X, Miao Y, Pu K. Reaction-based semiconducting polymer nanoprobes for photoacoustic imaging of protein sulfenic acids. ACS Nano. 2016; 11: 358-67.
4. Lyu Y, Xie C, Chechetka SA, Miyako E, Pu K. Semiconducting polymer nanobioconjugates for targeted photothermal activation of neurons. J Am Chem Soc. 2016; 138: 9049-52.
5. Pu K, Shuhendler AJ, Jokerst JV, Mei J, Gambhir SS, Bao Z, et al. Semiconducting polymer nanoparticles as photoacoustic molecular imaging probes in living mice. Nat Nanotechnol. 2014; 9: 233-9.
6. Nie L, Chen X. Structural and functional photoacoustic molecular tomography aided by emerging contrast agents. Chem Soc Rev. 2014; 43: 7132-70.
7. Jiang Y, Cui D, Fang Y, Zhen X, Upputuri PK, Pramanik M, et al. Amphiphilic semiconducting polymer as multifunctional nanocarrier for fluorescence/photoacoustic imaging guided chemo-photothermal therapy. Biomaterials. 2017; 145: 168-77.
8. Yin C, Zhen X, Zhao H, Tang Y, Ji Y, Lyu Y, et al. Amphiphilic semiconducting oligomer for near-infrared photoacoustic and fluorescence imaging. ACS Appl Mater Interfaces. 2017; 9: 12332-9.
9. Song J, Yang X, Yang Z, Lin L, Liu Y, Zhou Z, et al. Rational design of branched nanoporous gold nanoshells with enhanced physico-optical properties for optical imaging and cancer therapy. ACS Nano. 2017; 11: 6102-13.
10. Zhen X, Zhang C, Xie C, Miao Q, Lim KL, Pu K. Intraparticle energy level alignment of semiconducting polymer nanoparticles to amplify chemiluminescence for ultrasensitive *in vivo* imaging of reactive oxygen species. ACS Nano. 2016; 10: 6400-9.
11. Levi J, Kothapalli SR, Ma T-J, Hartman K, Khuri-Yakub BT, Gambhir SS. Design, synthesis, and imaging of an activatable photoacoustic probe. J Am Chem Soc. 2010; 132: 11264-9.
12. Yin C, Tang Y, Li X, Yang Z, Li J, Li X, et al. A single composition architecture-based nanoprobe for ratiometric photoacoustic imaging of glutathione (GSH) in living mice. Small. 2018; 14: 1703400.
13. Liu Y, Wang S, Ma Y, Lin J, Wang HY, Gu Y, et al. Ratiometric photoacoustic molecular imaging for methylmercury detection in living subjects. Adv Mater. 2017; 29: 1606129.
14. Chen Q, Liang C, Sun X, Chen J, Yang Z, Zhao H, et al. H2O2-responsive liposomal nanoprobe for photoacoustic inflammation imaging and tumor theranostics via in vivo chromogenic assay. P Natl Acad Sci USA. 2017; 114: 5343-8.
15. Knox HJ, Hedhli J, Kim TW, Khalili K, Dobrucki LW, Chan J. A bioreducible N-oxide-based probe for photoacoustic imaging of hypoxia. Nat Commun. 2017; 8: 1794.
16. Chen Q, Liu X, Zeng J, Cheng Z, Liu Z. Albumin-NIR dye self-assembled nanoparticles for photoacoustic pH imaging and pH-responsive photothermal therapy effective for large tumors. Biomaterials. 2016; 98: 23-30.
17. Cao Z, Tong R, Mishra A, Xu W, Wong GC, Cheng J, et al. Reversible cell-specific drug delivery with aptamer-functionalized liposomes. Angew Chem Int Ed Engl. 2009; 48: 6494-8.
18. van Vlerken LE, Duan Z, Seiden MV, Amiji MM. Modulation of intracellular ceramide using polymeric nanoparticles to overcome multidrug resistance in cancer. Cancer Res. 2007; 67: 4843-50.
19. Lo A, Lin C-T, Wu H-C. Hepatocellular carcinoma cell-specific peptide ligand for targeted drug delivery. Mol Cancer Ther. 2008; 7: 579-89.
20. Hua L, Wang Z, Zhao L, Mao H, Wang G, Zhang K, et al. Hypoxia-responsive lipid-poly-(hypoxic radiosensitized polyprodrug) nanoparticles for glioma chemo-and radiotherapy. Theranostics. 2018; 8: 5088-105.
21. Karimi M, Ghasemi A, Zangabad PS, Rahighi R, Basri SMM, Mirshekari H, et al. Smart micro/nanoparticles in stimulus-responsive drug/gene delivery systems. Chem Soc Rev. 2016; 45: 1457-501.
22. Fleige E, Quadir MA, Haag R. Stimuli-responsive polymeric nanocarriers for the controlled transport of active compounds: concepts and applications. Adv Drug Deliv Rev. 2012; 64: 866-84.
23. Lee ES, Na K, Bae YH. Super pH-sensitive multifunctional polymeric micelle. Nano Lett. 2005; 5: 325-9.
24. Hou J-T, Ren WX, Li K, Seo J, Sharma A, Yu X-Q, et al. Fluorescent bioimaging of pH: from design to applications. Chem Soc Rev. 2017; 46: 2076-90.
25. Webb BA, Chimenti M, Jacobson MP, Barber DL. Dysregulated pH: a perfect storm for cancer progression. Nat Rev Cancer. 2011; 11: 671.
26. Han J, Burgess K. Fluorescent indicators for intracellular pH. Chem Rev. 2009; 110: 2709-28.
27. Lee MH, Kim JS, Sessler JL. Small molecule-based ratiometric fluorescence probes for cations, anions, and biomolecules. Chem Soc Rev. 2015; 44: 4185-91.
28. Jana A, Nguyen KT, Li X, Zhu P, Tan NS, Ågren H, et al. Perylene-derived single-component organic nanoparticles with tunable emission: Efficient anticancer drug carriers with real-time monitoring of drug release. ACS Nano. 2014; 8: 5939-52.
29. Lai J, Shah BP, Garfunkel E, Lee K-B. Versatile fluorescence resonance energy transfer-based mesoporous silica nanoparticles for real-time monitoring of drug release. ACS Nano. 2013; 7: 2741-50.
30. Ge Z, Liu S. Functional block copolymer assemblies responsive to tumor and intracellular microenvironments for site-specific drug delivery and enhanced imaging performance. Chem Soc Rev. 2013; 42: 7289-325.
31. Jo J, Lee CH, Kopelman R, Wang X. In vivo quantitative imaging of tumor pH by nanosonophore assisted multispectral photoacoustic imaging. Nat commun. 2017; 8: 471.
32. Miao Q, Lyu Y, Ding D, Pu K. Semiconducting oligomer nanoparticles as an activatable photoacoustic probe with amplified brightness for in vivo imaging of pH. Adv Mater. 2016; 28: 3662-8.
33. Zeng L, Ma G, Lin J, Huang P. Photoacoustic Probes for Molecular Detection: Recent Advances and Perspectives. Small. 2018; 14: 1800782.
34. Yang Z, Song J, Dai Y, Chen J, Wang F, Lin L, et al. Self-assembly of semiconducting-plasmonic gold nanoparticles with enhanced optical property for photoacoustic imaging and photothermal therapy. Theranostics. 2017; 7: 2177-85.
35. Lyu Y, Fang Y, Miao Q, Zhen X, Ding D, Pu K. Intraparticle molecular orbital engineering of semiconducting polymer nanoparticles as amplified theranostics for in vivo photoacoustic imaging and photothermal therapy. ACS Nano. 2016; 10: 4472-81.
36. Miao Q, Xie C, Zhen X, Lyu Y, Duan H, Liu X, et al. Molecular afterglow imaging with bright, biodegradable polymer nanoparticles. Nat biotechnol. 2017; 35: 1102.
37. Jiang Y, Pu K. Multimodal biophotonics of semiconducting polymer nanoparticles. Accounts chem res. 2018; 51: 1840-9.
38. Miao Q, Pu K. Organic Semiconducting Agents for Deep-Tissue Molecular Imaging: Second Near-Infrared Fluorescence, Self-Luminescence, and Photoacoustics. Adv Mater. 2018; 30(49 e):1801778.
39. Zhen X, Zhang J, Huang J, Xie C, Miao Q, Pu K. Macrotheranostic Probe with Disease-Activated Near-Infrared Fluorescence, Photoacoustic, and Photothermal Signals for Imaging-Guided Therapy. Angew Chem Int Ed Engl. 2018; 130: 7930-4.
40. Jiang Y, Li J, Zhen X, Xie C, Pu K. Dual-Peak Absorbing Semiconducting Copolymer Nanoparticles for First and Second Near-Infrared Window Photothermal Therapy: A Comparative Study. Adv Mater. 2018; 30: 1705980.

41. Lyu Y, Zeng J, Jiang Y, Zhen X, Wang T, Qiu S, et al. Enhancing both biodegradability and efficacy of semiconducting polymer nanoparticles for photoacoustic imaging and photothermal therapy. ACS nano. 2018; 12: 1801-10.
42. Zhu H, Fang Y, Miao Q, Qi X, Ding D, Chen P, et al. Regulating near-infrared photodynamic properties of semiconducting polymer nanotheranostics for optimized cancer therapy. ACS Nano. 2017; 11: 8998-9009.
43. Tang W, Yang Z, Wang S, Wang Z, Song J, Yu G, et al. Organic Semiconducting Photoacoustic Nanodroplets for Laser-Activatable Ultrasound Imaging and Combinational Cancer Therapy. ACS Nano. 2018; 12: 2610-22.
44. Cui C, Yang Z, Hu X, Wu J, Shou K, Ma H, et al. Organic semiconducting nanoparticles as efficient photoacoustic agents for lightening early thrombus and monitoring thrombolysis in living mice. ACS Nano. 2017; 11: 3298-310.
45. Fan Q, Cheng K, Yang Z, Zhang R, Yang M, Hu X, et al. Perylene-diimide-based nanoparticles as highly efficient photoacoustic agents for deep brain tumor imaging in living mice. Adv Mater. 2015; 27: 843-7.
46. Yang Z, Tian R, Wu J, Fan Q, Yung BC, Niu G, et al. Impact of semiconducting perylene diimide nanoparticle size on lymph node mapping and cancer imaging. ACS Nano. 2017; 11: 4247-55.
47. Aigner D, Borisov SM, Petritsch P, Klimant I. Novel near infra-red fluorescent pH sensors based on 1-aminoperylene bisimides covalently grafted onto poly (acryloylmorpholine). Chem Commun. 2013; 49: 2139-41.
48. Cheng W, Cheng H, Wan S, Zhang X, Yin M. Dual-stimulus-responsive fluorescent supramolecular prodrug for antitumor drug delivery. Chem Mater. 2017; 29: 4218-26.
49. Li X, Wang H, Schneider JA, Wei Z, Lai W-Y, Huang W, et al. Catalyst-free one-step synthesis of ortho-tetraaryl perylene diimides for efficient OPV non-fullerene acceptors. J Mater Chem C. 2017; 5: 2781-5.
50. Chen Q, Liu X, Chen J, Zeng J, Cheng Z, Liu Z. A self-assembled albumin-based nanoprobe for in vivo ratiometric photoacoustic pH imaging. Adv Mater. 2015; 27: 6820-7.
51. Gong H, Dong Z, Liu Y, Yin S, Cheng L, Xi W, et al. Engineering of multifunctional nano-micelles for combined photothermal and photodynamic therapy under the guidance of multimodal imaging. Adv Funct Mater. 2014; 24: 6492-502.
52. Cheng L, He W, Gong H, Wang C, Chen Q, Cheng Z, et al. PEGylated micelle nanoparticles encapsulating a non-fluorescent near-infrared organic dye as a safe and highly-effective photothermal agent for in vivo cancer therapy. Adv Funct Mater. 2013; 23: 5893-902.
53. Dai J, Lin S, Cheng D, Zou S, Shuai X. Interlayer-crosslinked micelle with partially hydrated core showing reduction and pH dual sensitivity for pinpointed intracellular drug release. Angew Chem Int Ed Engl. 2011; 50: 9404-8.